Journal of Orthopaedic Translation 23 (2020) 89–100

Contents lists available at ScienceDirect

Journal of Orthopaedic Translation

journal homepage: www.journals.elsevier.com/journal-of-orthopaedic-translation

Original Article

Three-dimensional printed multiphasic scaffolds with stratified cell-laden gelatin methacrylate hydrogels for biomimetic tendon-to-bone interface engineering

Yi Cao [a], Shengbing Yang [b], Danyang Zhao [a], Yun Li [a], Sou San Cheong [a], Dong Han [a,**], Qingfeng Li [a,*]

[a] Department of Plastic and Reconstructive Surgery, Shanghai Ninth People's Hospital, Shanghai Jiao Tong University School of Medicine, Shanghai, China
[b] Shanghai Key Laboratory of Orthopaedic Implants, Department of Orthopaedic Surgery, Shanghai Ninth People's Hospital, Shanghai Jiao Tong University School of Medicine, Shanghai, China

ARTICLE INFO

Keywords:
3D printing
Enthesis
Gelatin methacrylate
Multiphasic scaffold
Tendon-to-bone interface engineering

ABSTRACT

Background: The anatomical properties of the enthesis of the rotator cuff are hardly regained during the process of healing. The tendon-to-bone interface is normally replaced by fibrovascular tissue instead of interposition fibrocartilage, which impairs biomechanics in the shoulder and causes dysfunction. Tissue engineering offers a promising strategy to regenerate a biomimetic interface. Here, we report heterogeneous tendon-to-bone interface engineering based on a 3D-printed multiphasic scaffold.

Methods: A multiphasic poly(ε-caprolactone) (PCL)–PCL/tricalcium phosphate (TCP)–PCL/TCP porous scaffold was manufactured using 3D printing technology. The three phases of the scaffold were designed to mimic the graded tissue regions in the tendon-to-bone interface—tendon, fibrocartilage, and bone. Fibroblasts, bone marrow–derived mesenchymal stem cells, and osteoblasts were separately encapsulated in gelatin methacrylate (GelMA) and loaded seriatim on the relevant phases of the scaffold, by which a cells/GelMA-multiphasic scaffold (C/G-MS) construct, replicating the native interface, was fabricated. Cell proliferation, viability, and chondrogenic differentiation were evaluated *in vitro*. The C/G-MS constructs were further examined to determine the potential of regenerating a continuous interface with gradual transition of teno-, fibrocartilage- and osteo-like tissues *in vivo*.

Results: In vitro tests confirmed the good cytocompatibility of the constructs. After seven days in culture, cellular microfilament staining indicated that not only could cells well proliferate in GelMA hydrogels but also efficiently attach to and grow on scaffold fibres. Moreover, by immunolocalizing collagen type II, chondrogenesis was identified in the intermediate phase of the C/G-MS construct that had been treated with transforming growth factor β3 for 21 days. After subcutaneous implantation in mice, the C/G-MS construct exhibited a heterogeneous and graded structure up to eight weeks, with distinguished matrix distribution observed at one week. Overall, gene expression of tenogenic, chondrogenic, and osteogenic markers showed increasing patterns for eight weeks. Among them, expression of collagen type X gene was found drastically increasing during eight weeks, indicating progressive formation of calcifying cartilage within the constructs.

Conclusion: Our findings demonstrate that the stratified manner of fabrication based on the 3D-printed multiphasic scaffold is an effective strategy for tendon-to-bone interface engineering in terms of efficient cell seeding, chondrogenic potential, and distinct matrix deposition in varying phases.

The translational potential of this article: We fabricated a biomimetic tendon-to-bone interface by using a 3D-printed multiphasic scaffold and adopting a stratified cell-seeding manner with GelMA. The biomimetic interface might have applications in tendon-to-bone repair in the rotator cuff. It can not only be an alternative to a biological fixation device but also offer an *ex vivo* living graft to replace the damaged enthesis.

* Corresponding author. Department of Plastic and Reconstructive Surgery, Shanghai Ninth People's Hospital, Shanghai Jiao Tong University School of Medicine, 19/F, No. 1 Building, 639 Zhi Zao Ju Road, Shanghai, 200011, PR China.
** Corresponding author. Department of Plastic and Reconstructive Surgery, Shanghai Ninth People's Hospital, Shanghai Jiao Tong University School of Medicine, 17/F, No. 1 Building, 639 Zhi Zao Ju Road, Shanghai, 200011, PR China.
E-mail addresses: evacao0102@yahoo.com (Y. Cao), bioshengbingy@163.com (S. Yang), Herion0830@sjtu.edu.cn (D. Zhao), liyun117@hotmail.com (Y. Li), susancheong0702@hotmail.com (S.S. Cheong), handong12000@163.com (D. Han), dr.liqingfeng@shsmu.edu.cn (Q. Li).

https://doi.org/10.1016/j.jot.2020.01.004
Received 14 November 2019; Received in revised form 18 December 2019; Accepted 13 January 2020
Available online 8 February 2020

Introduction

Rotator cuff tears are common conditions caused by acute injuries or chronic degenerative disorders. Surgical repairs are routinely performed and augmented by various approaches [1,2]. However, the complexity of the enthesis in the rotator cuff poses significant challenges for anatomical and functional restoration. It was reported that the re-tear rate after surgery was approximately 20–90% [3,4]. The tendon-to-bone interface is a typical fibrocartilaginous insertion, consisting of four distinct yet continuous tissue regions: tendon, fibrocartilage, mineralized fibrocartilage, and bone [5,6]. The compliant tendon properly connects the hard bone through a fibrocartilaginous zone, by which a functionally graded insertion is formed. This fibrocartilaginous insertion serves critical function in alleviating stress concentration during load transfer from the tendon to bone. Previous studies have demonstrated that, instead of regenerating fibrocartilage, the healing process was usually achieved by the formation of fibrovascular scar tissue [7,8]. Hence, the biomechanical properties of the native tendon-to-bone interface are hardly regained after injury.

Owing to poor outcomes of surgical repairs, researchers have begun to explore the feasibility of developing a biomimetic interface [9]. It can not only be an alternative to a biological fixation device but also offer an *ex vivo* living graft to replace the damaged enthesis. Tissue engineering exhibits a promising strategy to reach the goal [10]. In the musculoskeletal system, unlike numerous investigations pertinent to the osteochondral interface [11,12], fewer studies focus on the tendon-to-bone interface. To engineer soft and hard tissues simultaneously, the scaffold structure is considered to be the most essential design input. However, to date, there has been lack of optimized scaffolds that can both recapitulate the heterogeneous complex and meet the adequate mechanical needs [8,9,13,14]. Most investigations focused on biomimetic patches [2], which were unable to fulfil the need of repair in severe cases with massive loss of tendon or bone tissue. Three-dimensional (3D) printing, a rapidly developing technology of additive manufacturing, has emerged as an alternative method to produce tissue engineering scaffolds [15,16]. The unique advantage of 3D printing is to create a predesigned scaffold with customized structures in a layer-by-layer fashion. Using 3D printing, scaffold delamination could be avoided to a large extent. Besides, 3D-printed porous scaffolds with controllable pore sizes provide a better microenvironment for cell growth. The multihead printing system also allows multiple printing materials being used jointly. As for printing material, poly(ε-caprolactone) (PCL) exhibits excellent biocompatibility and biomechanical properties; therefore, it is a material applicable for tendon regeneration [17,18]. However, there is no osteoinductivity in PCL so that mineral additives are usually added into PCL for bone tissue engineering [19]. Tricalcium phosphate (TCP) is one of the typical additives owing to its inherent osteoinductivity and suitable degradation time [20,21].

Cells are important element in tissue engineering [10]. Main cell types present in the native tendon-to-bone interface are tendon fibroblasts (FBs), fibrochondrocytes, and osteoblasts (OBs). According to the literature, the cell source for tendon-to-bone interface engineering can be chosen in the following combinations [7,22,23]: (1) coculture of terminally differentiated cells, mainly FBs and OBs, with or without chondrocytes; (2) multipotent stem cells, such as bone marrow–derived mesenchymal stem cells (BMSCs), adipose-derived stem cells, or ligament/tendon/periosteal-derived progenitor/stem cells; (3) coculture of differentiated cells together with stem cells as stem cells is considered to be the most promising seed cells for cartilage tissue engineering. To choose stem cells alone, the scaffold should be equipped with regional biochemical or mechanical cues to induce gradient cell differentiation spatially. However, this strategy requires a comprehensive understanding of enthesis development, and so far, the lack of profound discoveries has made the design goal hard to reach [9,13]. Given the feasibility of producing multiphasic scaffolds, the coculture of differentiated cells together with stem cells is assumed to be a preferable strategy to mimic the fibrocartilaginous insertion, which might also unravel how the differentiation of stem cells is being influenced by heterotypic cellular interactions [22,24].

Cell seeding is a key step in tissue engineering. Static seeding, which allows cells to directly attach on the scaffold and finally grow on it, has been commonly adopted by many researchers. However, the procedure becomes troublesome when it comes to seeding three or more cell types simultaneously. Even distribution of various cell types is hardly achieved, and cell loading capacity is usually low in the intermediate phases of a multiphasic scaffold [25]. To tackle the problem, we hypothesize that cell seeding of multiple cell types could be achieved by loading cell-laden hydrogels onto the scaffolds in a stratified pattern. Gelatin methacrylate (GelMA) is a photocurable hydrogel developed from gelatin [26]. Owing to its remarkable cell responsiveness, biodegradability, and fast cross-linking ability, GelMA has been widely used for cellular encapsulation [27,28] and might be an ideal candidate hydrogel for stratified cell seeding.

In this study, we aim to fabricate a biomimetic tendon-to-bone interface based on a 3D-printed multiphasic scaffold. FBs, BMSCs, and OBs were separately seeded on relevant phases of the scaffold to regenerate teno-, fibrocartilage-, and osteo-like tissues. We developed a facile method to seed different cells on relevant phases of the scaffold by cross-linking cell-laden GelMA. Herein, we present the process of fabrication and ultimate structure of the biomimetic tendon-to-bone interface. *In vitro* biocompatibility and chondrogenesis of the fabricated constructs as well as *in vivo* regenerative potential of the heterogeneous interface after ectopic implantation in mice were further investigated (Figure 1A).

Materials and methods

Scaffold preparation

Scaffold design

The scaffold was scheduled to comprise three continuous phases representing tendon, fibrocartilage, and bone. A 0/90° lay-down pattern was used in the top (bone) and bottom (tendon) phases. Fibrocartilage is an avascular tissue with isolated fibrochondrocytes in lacunae embedded in the extracellular matrix (ECM). Therefore, the intermediate (fibrocartilage) phase was designed to consist of four layers depositing in a uniform rectangular wavelike pattern. This particular deposition pattern would eventually form four ducts with ample space for containing ECM-mimicking hydrogels and leave one opening of each duct for facile filling of hydrogels (Figure 2A).

Three-dimensional printing

A 3D-Bioplotter® Manufacturer Series printer (EnvisionTEC, Gladbeck, Germany) with a multihead deposition system was used. Perfactory Software Suite 3.2 (EnvisionTEC) was used to monitor and manage the printing process. PCL and TCP were purchased from Sigma-Aldrich (St. Louis, MO, USA). For the bottom (tendon) phase, PCL pellets were directly added into the steel chamber, heated up to 160 °C for complete meltdown, and turned into printable liquid. For top (bone) and intermediate (fibrocartilage) phases, PCL pellets were dissolved in dichloromethane for 1.5 h. After that, TCP particles, in an equivalent weight of PCL (PCL:TCP = 50:50), were added into the PCL solution by vigorously stirring to form homogeneous blends. When the viscosity was appropriate for printing, the PCL/TCP composite was fed into the chamber in a working temperature of 25 °C. During the process of printing, the polymer fibres were extruded through nozzles of 300-μm diameter. Printing speeds were empirically set to 3 mm/s for PCL deposition and 5–8 mm/s for PCL/TCP deposition. Finally, the PCL–PCL/TCP–PCL/TCP porous scaffold, with dimensions of 8 mm × 8 mm × 2.5 mm (Figure 2B), was manufactured in a layer-by-layer fashion from tendon (PCL, two layers), fibrocartilage (PCL/TCP, four layers) to bone (PCL/TCP, three layers) phases in *z*-direction. All printed scaffolds were dried at 37 °C and sterilized using ^{60}Co γ-irradiation.

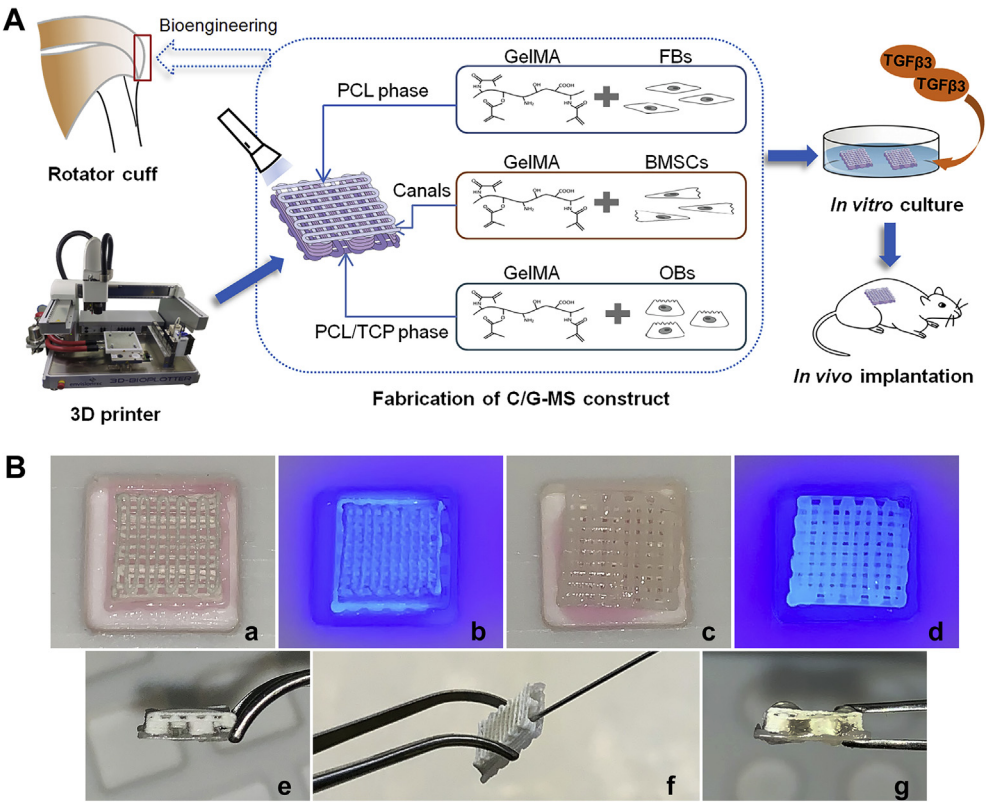

Figure 1. (A) Illustration of the study design. (B) Photographs showing fabrication of the C/G-MS construct. FBs/GelMA was loaded on the PCL phase (a) and cross-linked under 405-nm visible light (b). Then, OBs/GelMA was loaded on the PCL/TCP phase and cross-linked (c and d). BMSCs/GelMA was injected into intermediate ducts (f) followed by cross-linking. Lateral views showing ducts before (e) and after injection (g). 3D = three-dimensional; BMSCs = bone marrow–derived mesenchymal stem cells; C/G-MS = cells/GelMA-multiphasic scaffold; FBs = fibroblasts; GelMA = gelatin methacrylate; OBs = osteoblasts; PCL = poly(ε-caprolactone); TCP = tricalcium phosphate; TGFβ3 = transforming growth factor β3.

Scaffold characterization

The structure of 3D-printed scaffolds was observed by micro-computed tomography (microCT; SCANCO, Bassersdorf, Switzerland). Three-dimensional images were reconstructed after scanning the samples at an isometric resolution of 10 μm. The surface microstructures of the PCL phase, PCL/TCP phase, and lateral of the scaffolds were demonstrated by scanning electron microscopy (SEM; HITACHI, Tokyo, Japan). The samples were coated by gold sputtering and examined by SEM at an electron acceleration of 3.0 kV. Surface wettability of the PCL and PCL/TCP phases was separately assessed by measuring the static contact angles using the sessile drop method. *In vitro* degradation was carried out by incubating the scaffolds in the simulated body fluid (SBF) at 37 °C for 28 days. The weight-average molecular weight of the scaffolds and *pH* value of the SBF were measured along degradation. Before and after incubation in SBF for 7, 14, and 28 days, biomechanical tests were conducted using a mechanical testing machine (Instron, Norwood, MA, USA). The samples were fixed and compressed to 70% deformation, and the compressive modulus was calculated to evaluate the compression bearing capacity of the scaffolds.

Cell isolation and expansion

Two-week-old C57BL/6 mice (male, weighing 8 g) were used for primary cultures. Animal experiments were approved by the Animal Ethics Committee of Shanghai Ninth People's Hospital. In brief, for isolation of FBs, Achilles tendons were cut into small pieces and digested with 3 mg/mL collagenase type I (Gibco, Grand Island, NY, USA) and 4 mg/mL dispase (Roche, Basel, Switzerland) [29]. Single-cell suspension was obtained and cultured with Dulbecco's Modified Eagle's medium (DMEM) (Gibco), supplemented with 10% fetal bovine serum (Gibco), 100 U/mL penicillin, and 100 μg/mL streptomycin (Gibco). For isolation of OBs, the calvaria was cut into small fragments, followed by sequential enzymatic digestion using 2 mg/mL collagenase type II (Gibco) and 0.25% trypsin–EDTA (Gibco). Then, the bone fragments were transferred into flasks and cultured with the growth media as described previously, awaiting migration of osteo cells from the matrix [30]. For isolation of BMSCs, the bone marrow cavity was exposed, and marrow cells were collected in a culture dish by flushing the bone marrow with growth media using a syringe. Media were further added for cell attachment and growth [31]. All cell cultures were kept at 37 °C in a humidified atmosphere containing 5% CO_2. Media were changed every three days. Once reaching subconfluency, the primary cultures were treated with trypsin for passaging. Cells from passages two and three were used in this study.

Fabrication of cell–scaffold constructs

Before cell seeding, the 3D-printed scaffolds were incubated in growth media at 37 °C overnight and then dried. Meanwhile, GelMA solution was prepared by dissolving the lyophilized GelMA (EFL, Suzhou, China) in DMEM. Lithium phenyl-2,4,6-trimethylbenzoylphosphinate (LAP) was added as a visible-light cross-linking initiator. GelMA at low concentrations (<5% w/v) exhibits outstanding biocompatibility [32]. In the pilot study, final concentrations of GelMA and LAP were determined to be 5% w/v and 0.1% w/v, respectively. FBs, OBs, and BMSCs were separately suspended in GelMA solution, each of them forming a cell density of 1×10^6/mL for *in vitro* tests or 1×10^7/mL for *in vivo* tests. The fabrication commenced from the tendon and bone phases (Figure 1B). Initially, 60 μL of the FBs/GelMA solution was pipetted into a 10 mm × 10 mm square mould. The PCL phase was faced downwards and quickly immersed in the solution. The cross-linking of GelMA was immediately induced under 405-nm wavelength light for 20 s. Then, in another square mould, the same amount of OBs/GelMA was loaded onto the PCL/TCP phase in the same way. For the intermediate phase, 100 μL of the BMSCs/GelMA solution was directly injected into the ducts through the openings on one lateral of the scaffold using a 1-mL syringe, followed by photocrosslinking immediately. Then, another 100 μL of the BMSCs/GelMA solution was injected and cross-linked in the ducts on the other lateral. Finally, fabrication of the cells/GelMA-multiphasic scaffold (C/G-MS) construct was completed.

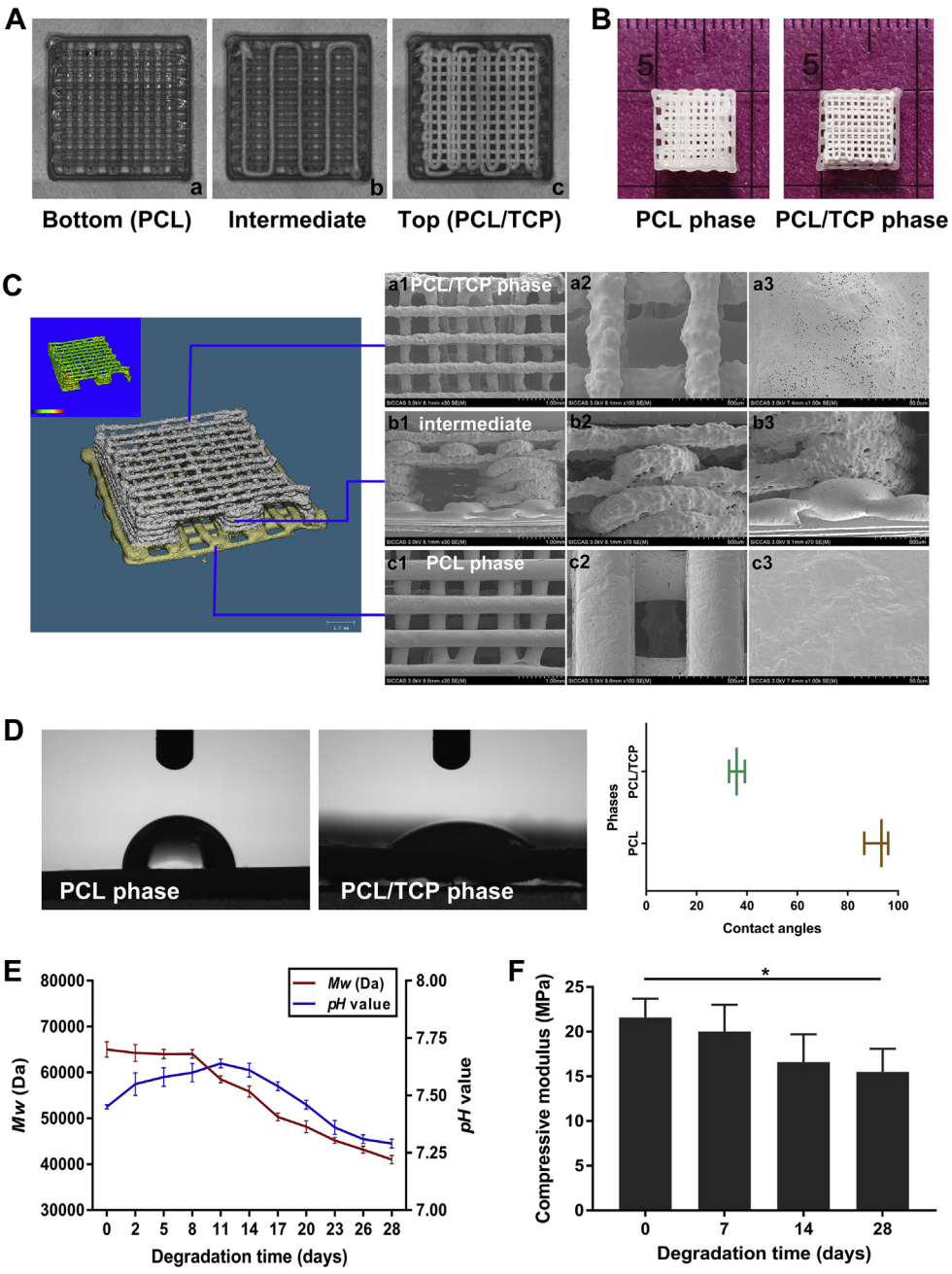

Figure 2. (A) Real-time images taken using 3D printing software during the bottom-up printing process, showing the 0/90°(a and c) and rectangular wavelike lay-down patterns (b). (B) Morphology and size of the 3D-printed scaffold. (C) MicroCT (left) demonstrated print quality and the predesigned structure. SEM micrographs (right) displaying surface microstructures of the PCL/TCP phase (a1∼a3), intermediate ducts (b1∼b3), and PCL phase (c1∼c3). (D) Contact angles separately obtained from PCL and PCL/TCP phases using the sessile drop method. (E) Changes in weight-average molecular weight (*Mw*) of the scaffolds and *pH* value of the incubation medium. (F) Compressive modulus of the scaffolds during 28 days of degradation. Data are mean ± SD. $^*p < 0.05$. 3D = three-dimensional; microCT = micro-computed tomography; PCL = poly(ε-caprolactone); SD = standard deviation; SEM = scanning electron microscopy; TCP = tricalcium phosphate.

Cytocompatibility tests

Cell viability was evaluated using the Live and Dead Cell Double Staining Kit (Abbkine, Wuhan, China) after being cultured for one, four, and seven days ($n = 3$). The kit contains a cell-permeable green fluorescent LiveDye and a nonpermeable red fluorescent NucleiDye. On evaluation, at all time points, the C/G-MS constructs were incubated in the assay dye at 37 °C for 30 min and visualized by confocal laser scanning microscopy (CLSM; Nikon, Tokyo, Japan). Cell viability was calculated by randomly choosing five regions for each sample. The PCL and PCL/TCP phases were separately evaluated and compared.

Cell proliferation was investigated using the Cell Counting Kit-8 (CCK-8) assay (Dojindo, Kumamoto, Japan). After fabrication of the C/G-MS constructs, the FBs/GelMA, BMSCs/GelMA, and OBs/GelMA solutions in the same amount as in the C/G-MS constructs were added and gelated seriatim in the same well of a 48-well culture plate. Thus, the cells/GelMA hydrogels were fabricated and served as controls. After one, four, and seven days in culture, both C/G-MS constructs ($n = 3$) and cells/GelMA hydrogels ($n = 3$) were incubated in CCK-8 solution for 4 h. Then, 10 μL of the supernatant was transferred to a 96-well culture plate, and its absorbance at 450 nm was read using a microplate reader (BioTek, Winooski, VT, USA).

Actin-Tracker Green (Beyotime, Shanghai, China), a solution of phalloidin conjugated with fluorescein isothiocyanate (FITC), was used for microfilament staining to visualize cell morphology in the C/G-MS coculture system. After seven days in culture, the C/G-MS constructs ($n = 3$) were fixed in 4% paraformaldehyde for 1 h. The cells were permeabilized with 0.1% Triton X-100 for 40 min, blocked with 2.5% bovine serum albumin (BSA), and stained with Actin-Tracker Green for 2 h at room temperature. The nuclei were subsequently stained with 4',6-diamidino-2-phenylindole (DAPI) (Beyotime) for another 7 min. The cytoskeleton and the nuclei of the cells growing in the constructs were visualized by CLSM.

In vitro chondrogenesis

Chondrogenesis was examined by immunocytochemistry (ICC) analysis. The C/G-MS constructs ($n = 3$) were cultured in DMEM supplemented with 50 mg/mL insulin–transferrin–sodium selenite plus, 100 μg/mL sodium pyruvate, 40 μg/mL proline, 0.1 μM dexamethasone, and 50 μg/mL ascorbate [33]. Recombinant human transforming growth factor β3 (TGFβ3; PeproTech, Rocky Hill, NJ, USA) was added into the supplemented media at a final concentration of 10 ng/mL. Meanwhile, the C/G-MS constructs cultured without the addition of TGFβ3 served as controls ($n = 3$). Media were changed every three days. After 21 days of induction, the lateral sides of the C/G-MS constructs were cut off, and the remaining samples were fixed in 4% paraformaldehyde for 1 h. To immunolocalize the chondrogenic protein collagen type II (COL2), the cells were permeabilized with 0.5% Triton X-100 for 40 min and blocked with 5% goat serum for 1.5 h. Then, the constructs were incubated with the primary antibody anti-collagen II (1/100, ab34712; Abcam, Cambridge, MA, USA) at 4 °C overnight. An Alexa Fluor® 488-conjugated goat anti–rabbit IgG (1/500, ab150081; Abcam) was used as the secondary antibody. After 3 h of incubation with the secondary antibody, the nuclei were stained with 1 μg/mL Hoechst 33342 (H1399, Thermofisher, Waltham, MA, USA) for 15 min. The expression of COL2 within the constructs was observed by CLSM.

C/G-MS construct implantation in mice

The C/G-MS constructs were prefabricated one day before animal studies. Before fabrication, BMSCs were cultured for 21 days in chondrogenic induction media with the addition of TGFβ3. Twenty-seven 5-week-old C57BL/6 mice (male, weighing 20 g) were adopted for *in vivo* tests. Under sterile conditions, the mice were anesthetized with 1% pentobarbital sodium (100 mg/kg) through intraperitoneal injection. A 1-cm-long incision was made on the left or right side of dorsal skin, and a subcutaneous pocket was created. The C/G-MS constructs were then randomly implanted in the subcutaneous pockets. For histological studies, the C/G-MS constructs were cut into half size and implanted on the left dorsum, whereas cell-free blank scaffolds in the same size were implanted on the right dorsum, which served as controls. After surgery, all mice were allowed to eat and drink *ad libitum*. No severe complications occurred. On evaluation, at all time points, the mice were sacrificed, and the samples were harvested for further investigations.

Expression of tendon-to-bone interface–related genes

The mRNA expression of tendon-to-bone interface–related genes of the implanted C/G-MS constructs was determined by real-time quantitative polymerase chain reaction (qPCR). Candidate genes included the tenogenic marker Scleraxis (*Scx*), the osteogenic marker runt-related transcription factor 2 (*Runx2*), and chondrogenic markers collagen type II (*Col2*), aggrecan (*Agg*), sex-determining region Y-box 9 (*Sox9*), and collagen type X (*Col10*). At postsurgical one, four, and eight weeks, the implanted samples ($n = 6$) were harvested and homogenized with liquid nitrogen. Total RNA was extracted using TRIzol (Invitrogen, Carlsbad, CA, USA) and transcripted to complementary DNA (cDNA) using the PrimeScript™ RT Master Mix (TaKaRa, Tokyo, Japan). The primers were designed based on the Genbank database and synthesized to amplify candidate genes (Table 1). Real-time qPCR was performed using the Real-time PCR System (ABI, Foster City, CA, USA) using the TB Green® Premix Ex Taq™ kit (TaKaRa). Expression of the candidate genes was normalized to that of the glyceraldehyde 3'-phosphate dehydrogenase (GAPDH) gene, which served as an internal control.

Histological and immunohistochemical staining

At one, four, and eight weeks after implantation, the C/G-MS constructs ($n = 3$) were harvested from the left dorsum, and the cell-free scaffolds ($n = 3$) were harvested from the right dorsum. All scaffolds and their surrounding soft tissues were fixed in 4% paraformaldehyde for 48 h. The samples were embedded in paraffin under standard histological procedures and sectioned perpendicular to the duct on the lateral at a thickness of 4 μm. The sections were stained with haematoxylin and eosin (H&E) to assess morphology and inflammatory changes. The sections were also stained with Masson's trichrome (MT), toluidine blue (TB), and safranin O (SO)/fast green (FG) to examine collagen production, chondrogenesis, and osteogenesis.

The deposition of collagen type I (COL1) and COL2 was determined by immunohistochemical (IHC) staining. The sections were incubated with primary antibodies anti-collagen I (1/100, ab34710; Abcam) or anti-collagen II (1/50, ab34712; Abcam) at 4°C overnight.. After that, a horseradish peroxidase (HRP)-conjugated secondary antibody goat anti-rabbit IgG (1/20000, ab205718; Abcam) was used to detect the primary antibodies. Besides, the sections of the surrounding soft tissues were stained with primary anti-CD68 (1/200, ab125212; Abcam) to evaluate phagocytic activities of macrophages. Finally, all sections were added with 3,3′-diaminobenzidine (DAB) and counterstained with haematoxylin. Images were obtained by light microscopy (Nikon). The COL1-, COL2-, and CD68-positive areas were calculated.

Statistical analysis

The data were expressed as mean ± standard deviation. One-way analysis of variance and *post hoc* least significant difference tests were performed to analyze the data and determine the level of significance. Statistical differences were considered significant at $p < 0.05$ and highly significant at $p < 0.01$. Data analyses were conducted using SPSS version 19.0 software (IBM, Armonk, NY, USA).

Results

Scaffold characterization

As demonstrated in Figure 2, the 3D-printed scaffolds were manufactured as designed and showed homogeneous size and density. The structure and surface morphology of the scaffolds were examined by microCT and SEM. Porosities of the top and bottom phases were 78.2 ± 0.1% and 59.3 ± 0.4%, respectively. The intermediate phase was composed of four parallel ducts, each of them having one opening. SEM

Table 1
Primer sequences used for real-time qPCR analysis.

Gene	Forward: 5′–3′	Reverse: 5′–3′	Product size (bp)
Scx	CAAAGACCGTGACAGAAAGAC	CTCTCCGTGACTCTTCAGTG	111
Agg	CAAGGAAAAGGAGGTGGTACT	TCATTGGAGCGAAGGTTCT	144
Sox9	TCTGTGGGAGCGACAACTTTA	GGAGGGAGGGAAAACAGAGAA	104
Col2a1	AAGAGCAAGGAAAAGAAACACA	GACAGTAGACGGAGGAAAGTCA	128
Col10a1	AATACCCTTTCTGCTGCTAATG	TGCCTTGTTCTCCTCTTACTG	170
Runx2	GGACTGTGGTTACCGTCAT	GGAGGATTTGTGAAGACTGTT	172
GAPDH	CCCGTAGACAAAATGGTGAA	TGCCGTGAGTGGAGTCATAC	169

Agg = aggrecan; *Col2* = collagen type II; *Col10* = collagen type X; GAPDH = glyceraldehyde 3'-phosphate dehydrogenase; *Runx2* = runt-related transcription factor 2; *Scx* = Scleraxis; *Sox9* = sex-determining region Y-box 9; qPCR = quantitative polymerase chain reaction.

micrographs displayed three structurally varying yet continuous phases, with 100% interconnectivity. The areas between the two neighbouring phases displayed an integrated connection. By using the sessile drop method, the contact angles of PCL and PCL/TCP phases were separately measured as 92.0°±4.9° and 36.0°±3.2°, respectively, indicating a better surface wettability in the PCL/TCP phase than in PCL owing to hydrophilicity of TCP. We examined the *in vitro* degradation of the scaffolds in SBF for a 28-day period. The weight-average molecular weight of the scaffolds showed a descending trend along with degradation. The *pH* value had a slight increase in 11 days, followed by decreasing to approximate 7.3 at the end of four weeks. Compressive modulus slowly decreased by 28% along with degradation but was still measured as about 15.5 MPa on Day 28, suggesting the appropriate degradation rate and reliable mechanical properties of the 3D-printed scaffolds.

Cytocompatibility tests

In live/dead cell double staining, living cells and dead cells were labelled green and red, respectively. At one day after fabrication, the cells in the PCL and PCL/TCP phases were detected to be 91.7% ± 2.6% and 91.7% ± 2.7% viable, respectively. After seven days in culture, the cells in the PCL/TCP phase retained the viability of 91.4% ± 3.0%, whereas the cell viability in the PCL phase slightly decreased over time, but still as high as 89.2% ± 3.6% viable. Thus, nontoxicity of the scaffolds was identified in both phases. There was no significant difference in cell viability between PCL and PCL/TCP phases during seven days (Figure 3A–C).

The CCK-8 assay was used to assess cell proliferation *in vitro*. The absorbance values of the C/G-MS constructs at one, four, and seven days were 0.29 ± 0.01, 0.62 ± 0.09, and 1.13 ± 0.10, and those of the cells/GelMA hydrogels were 0.70 ± 0.01, 1.35 ± 0.05, and 1.52 ± 0.10, respectively. The linear increase of absorbance indicated that the cells exhibited an increase in proliferation in both groups during seven days. Although the trends in cell proliferation were consistent in both C/G-MS constructs and cells/GelMA hydrogels, the absorbance of the former was overall lower. Because the cell amounts were the same in both groups, the lower absorbance in C/G-MS might occur since some of the soluble formazan dye had been absorbed by the scaffold fibres in C/G-MS constructs during incubation (Figure 3D).

Actin filaments of the cytoskeleton were stained with FITC-phalloidin. CLSM revealed the cytoskeletal morphology of the cells growing in the C/G-MS constructs. During fabrication, the cells were loaded by GelMA onto the 3D-printed scaffold. After seven days in culture, some cells originally encapsulated in GelMA appeared to grow and proliferate on the surface of scaffold fibres. As shown in Figure 4A, the cells growing on the surface of scaffold fibres exhibited elongated, clustered, and multilayered morphologies with the extended spreading of actin filaments, whereas the cells within GelMA displayed heterogeneous and monolayered morphologies.

In vitro chondrogenesis

Chondrogenic induction of the C/G-MS constructs was accomplished using supplemented media with the addition of TGFβ3. After 21 days of induction culture, chondrogenesis was examined by ICC analysis, by which COL2 was fluorescently labelled green and detected by CLSM. In the C/G-

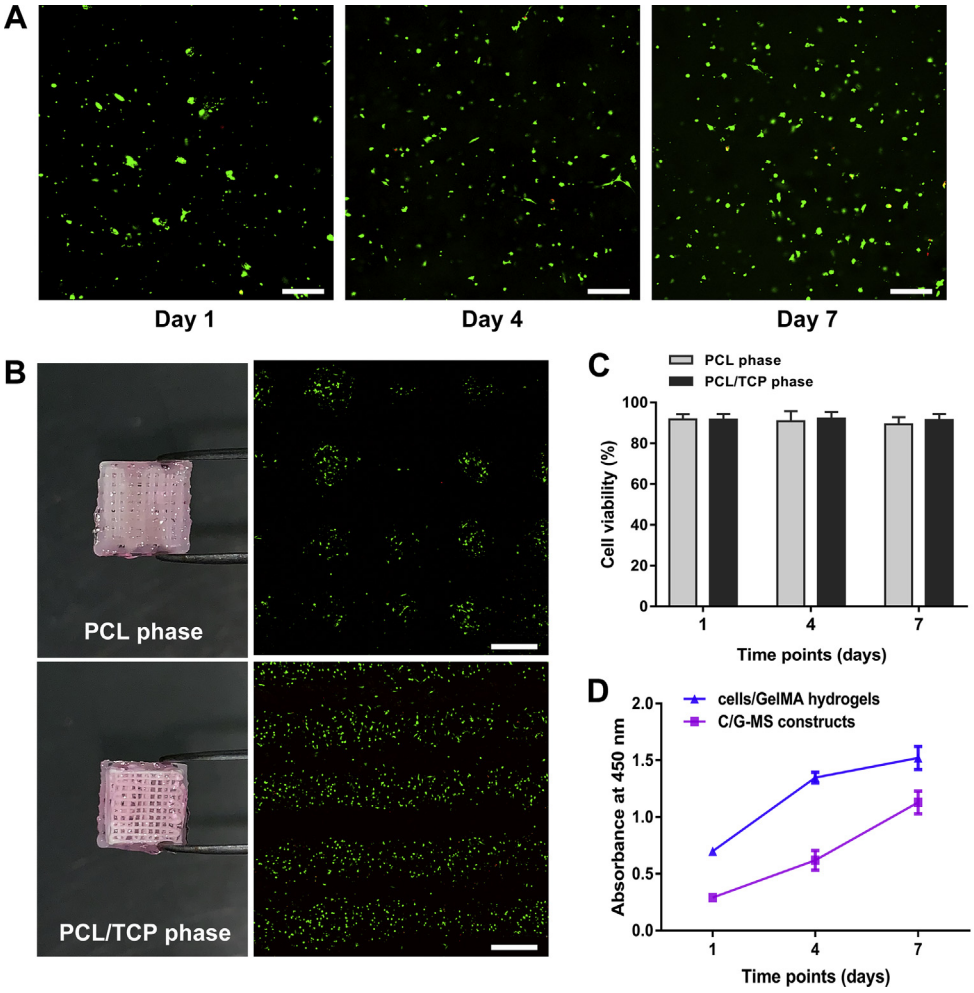

Figure 3. Cytocompatibility tests. (A) Representative images of live/dead cell double staining of the C/G-MS construct on Day 1, 4, and 7. Scale bars: 100 μm. (B) Live/dead cell staining of both PCL and PCL/TCP phases exhibited good cell viability at Day 7. Scale bars: 500 μm. (C) Cell viability of both PCL and PCL/TCP phases was mostly over 90% at all time points. No significant difference was noted between the two phases. (D) The Cell Counting Kit-8 (CCK-8) assay showed an increase in cell proliferation in both C/G-MS constructs and cells/GelMA hydrogels during seven days in culture. Data are mean ± SD. C/G-MS = cells/GelMA-multiphasic scaffold; GelMA = gelatin methacrylate; PCL = poly(ε-caprolactone); SD = standard deviation; TCP = tricalcium phosphate.

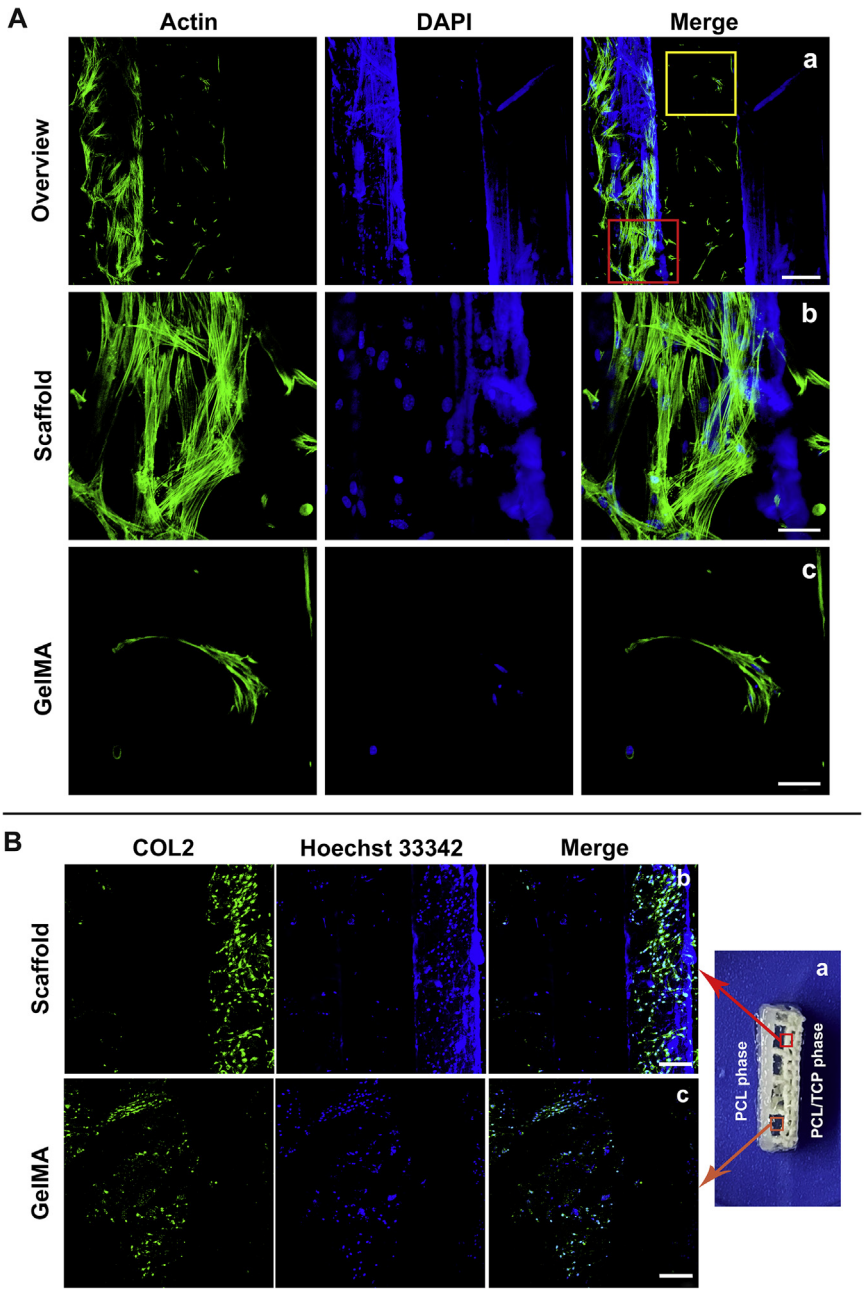

Figure 4. (A) Cellular actin staining in the C/G-MS constructs on Day 7. Red rectangle in (a) showing spreading of actin filaments in clustered cells on scaffold fibres (b), while yellow rectangle showing monolayered morphologies in GelMA (c). Scale bars: a, 200 μm; b and c, 50 μm. (B) Immunocytochemistry (ICC) analysis revealed chondrogenesis in C/G-MS constructs *in vitro*. COL2 emitting green fluorescence was detectable on the lateral of the intermediate phase (a), both on the surface of scaffold fibres (b) and in GelMA hydrogels (c). Scale bars: 200 μm. C/G-MS = cells/GelMA-multiphasic scaffold; GelMA = gelatin methacrylate; PCL = poly(ε-caprolactone); TCP = tricalcium phosphate; DAPI = 4',6-diamidino-2-phenylindole.

MS coculture system, with the addition of TGFβ3, expression of COL2 was visualized not only in GelMA hydrogels in the intermediate phase but also on the surface of scaffold fibres (Figure 4B). In contrast, no positive expression of COL2 could be observed in C/G-MS constructs of the control group without treating with TGFβ3 (see Supporting Information).

Expression of tendon-to-bone interface–related genes

After subcutaneous implantation in mice, changes in gene expression in C/G-MS constructs during eight weeks were measured by real-time qPCR (Figure 5). Relative quantitation of candidate gene expression normalized by GAPDH gene expression was used to determine the level of target gene expression. To assess chondrogenesis, expression of *Col2*, *Agg*, and *Sox9*, as well as the hypertrophic marker *Col10*, was examined. Gene expression of *Col2*, *Agg*, and *Sox9* exhibited a similar pattern of slight increase during eight weeks. However, there was no statistical difference in these changes, except that the expression of *Agg* was significantly increased at four weeks than at one week ($p < 0.01$). *Col10* is mainly synthesized by hypertrophic chondrocytes. An extremely low level of *Col10* expression was noted in the early period after implantation, whereas the expression increased drastically by approximately 30 times and 500 times at four and eight weeks, respectively ($p < 0.01$). Throughout implantation, the expression of the tenogenic marker *Scx* was significantly upregulated from one to eight weeks, with the highest expression at eight weeks ($p < 0.05$). Gene expression of the osteogenic marker *Runx2* peaked at four weeks and declined markedly after that. The level of Runx2 expression at four weeks was nearly three times that at Week 1 ($p < 0.01$) and two times that at Week 8 ($p < 0.05$).

Histological and IHC staining

Tissue distribution, collagen production, and proteoglycan synthesis of both C/G-MS and cell-free multiphasic scaffolds were examined at one, four, and eight weeks after implantation. In sections stained with H&E,

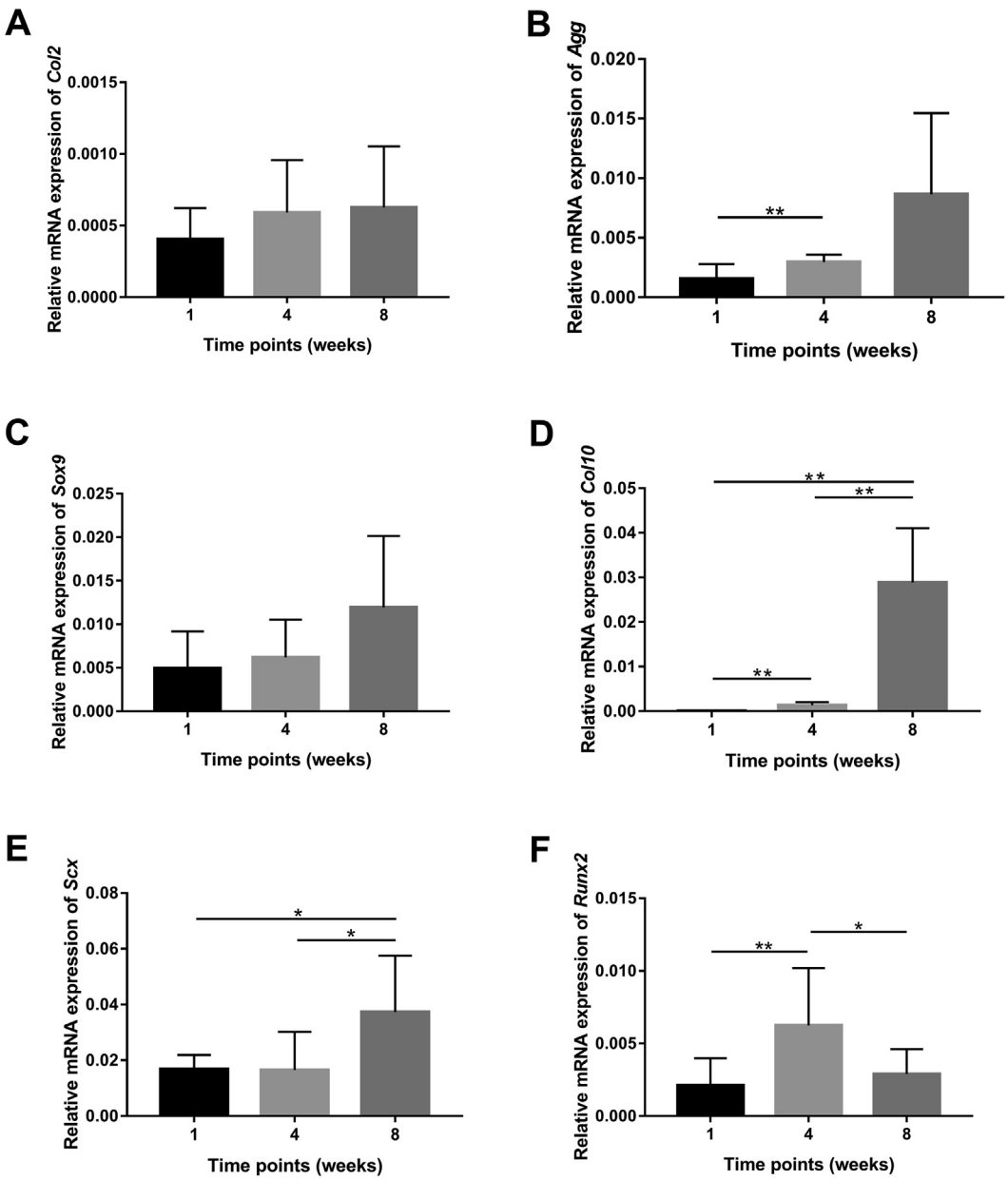

Figure 5. Real-time qPCR revealed mRNA expression levels of interface-related genes in the implanted C/G-MS constructs relative to the GAPDH gene at one, four, and eight weeks after surgery: (A) *Col2*: collagen type II; (B) *Agg*: aggrecan; (C) *Sox-9*: sex-determining region Y-box 9; (D) *Col10*: collagen type X; (E) *Scx*: Scleraxis; (F) *Runx2*: runt-related transcription factor 2. Data are mean ± SD. $*p < 0.05$, $**p < 0.01$. C/G-MS = cells/GelMA-multiphasic scaffold; GAPDH = glyceraldehyde 3'-phosphate dehydrogenase; GelMA = gelatin methacrylate; qPCR = quantitative polymerase chain reaction; SD = standard deviation.

we observed that the inflammatory cell infiltration in C/G-MS constructs peaked at one week and subsided drastically from four weeks. In contrast, the inflammatory changes in cell-free scaffolds were generally mild during eight weeks, only with discernible inflammatory infiltration adjacent to the scaffold fibres. H&E staining also revealed abundant tissue distribution in all phases of C/G-MS constructs from one to eight weeks. There was nearly no tissue ingrowth in cell-free scaffolds at Week 1; however, at Week 8, tissue distribution in the entire cell-free scaffolds was nearly similar to that in C/G-MS constructs. As shown in Figure 6, similar evident patterns of tissue integration in both scaffolds were identified by MT staining. Collagenous matrix stained as blue was abundant in all phases of C/G-MS constructs during eight weeks. On the contrary, few collagenous tissues could be observed in the cell-free scaffolds at one week; however, collagen production increased progressively up to eight weeks. Based on the morphology of endothelial cells and the amount of newly formed vessels shown in H&E and MT staining, neovascularization in both cell-seeded and cell-free scaffolds was found markedly increasing at four weeks. At eight weeks, more mature blood vessels inside the scaffolds were identified in both implants. TB and SO/FG staining methods confirmed the proteoglycan distribution in the intermediate (fibrocartilage) phase of the C/G-MS construct at one week after implantation. The staining subsided significantly from four to eight weeks, indicating less chondrocytes differentiated from BMSCs without sustained chondrogenic induction. SO/FG staining also exhibited slight green in the bone phase of C/G-MS constructs from four to eight weeks. At eight weeks, the PCL/TCP phase partially collapsed in both implants along with TCP degradation.

IHC staining further assessed collagen production and chondrocyte distribution within the C/G-MS constructs (Figure 7). IHC assay showed positive staining of COL1 in all phases of C/G-MS constructs during eight weeks, as well as in all phases of cell-free scaffolds at eight weeks. The results were in accordance with the findings of MT staining,

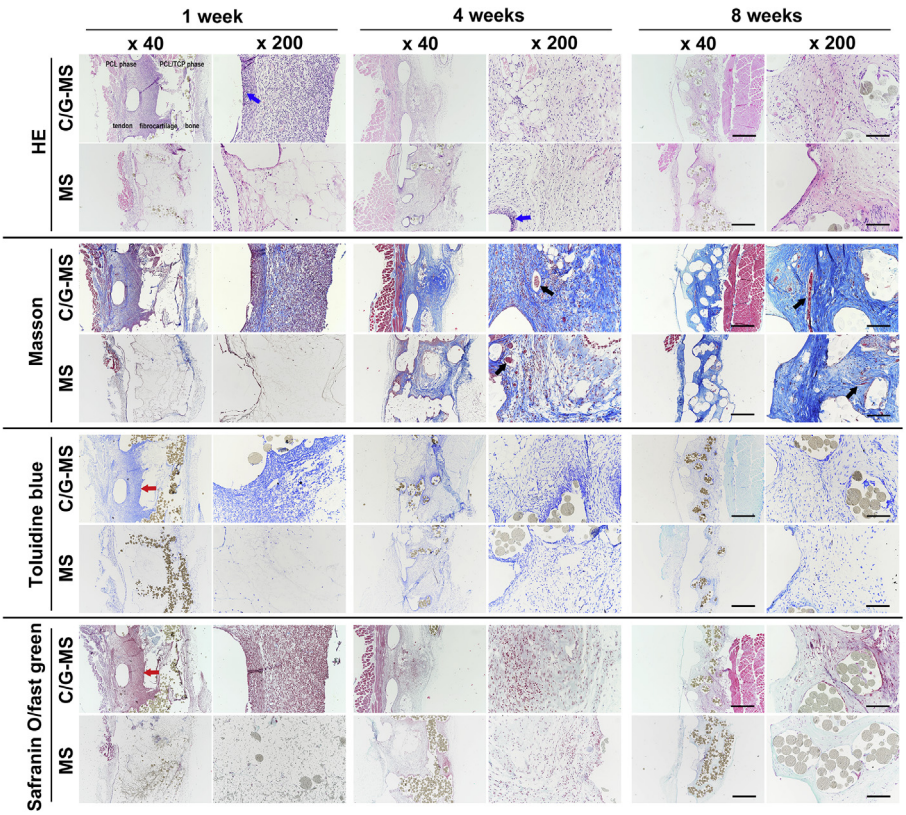

Figure 6. Representative histological images of C/G-MS constructs and cell-free multiphasic scaffolds (MS) at one, four, and eight weeks after implantation. Images are arrayed in a uniform direction with PCL phase in the left and the PCL/TCP phase in the right. Tissue integration and inflammatory infiltration were examined by haematoxylin and eosin (H&E) staining. Collagen deposition was confirmed by Masson's trichrome (MT) staining. Toluidine blue (TB) and safranin O (SO)/fast green (FG) staining demonstrated chondrogenesis and osteogenesis in C/G-MS constructs. Scaffolds partially collapsed at eight weeks. Blue arrows indicate inflammatory cell infiltration; black arrows indicate blood vessels; red arrows indicate cartilage formation in the intermediate phase. Scale bars: (×40), 500 μm; (×200), 100 μm. C/G-MS = cells/GelMA-multiphasic scaffold; GelMA = gelatin methacrylate; PCL = poly(ε-caprolactone); TCP = tricalcium phosphate.

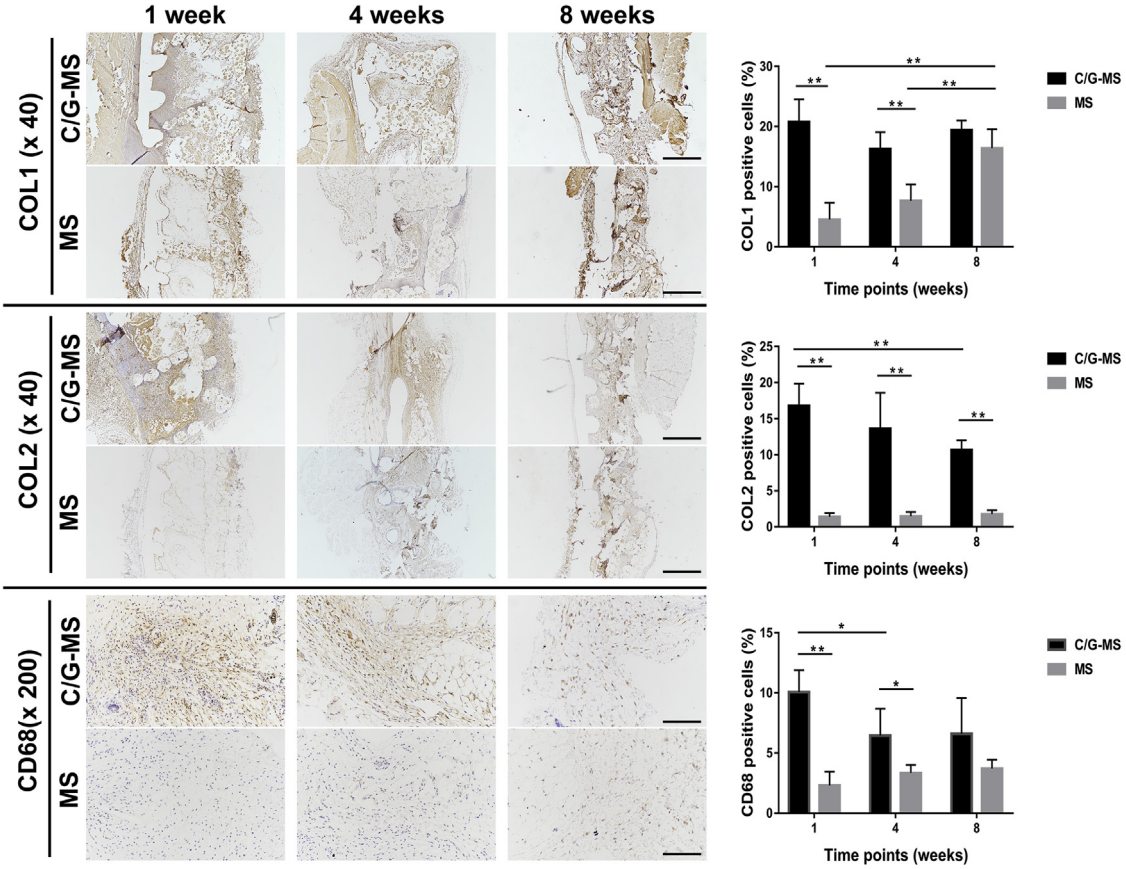

Figure 7. IHC staining revealed expression of collagen type I (COL1), collagen type II (COL2), and CD68 during eight weeks after implantation. Semiquantitative analysis was conducted and compared between C/G-MS constructs and cell-free scaffolds (*$p < 0.05$, **$p < 0.01$). Data are mean ± SD. Scale bars: (×40), 500 μm; (×200), 100 μm. C/G-MS = cells/GelMA-multiphasic scaffold; GelMA = gelatin methacrylate; IHC = immunohistochemical; SD = standard deviation.

demonstrating persistent collagen production in C/G-MS constructs and gradual ingrowth of collagen fibres in cell-free scaffolds. Semi-quantitative analysis of COL1 expression showed no significant difference between two implants at eight weeks, suggesting good biocompatibility of the 3D-printed scaffolds *in vivo*. Positive expression of the cartilage-related marker COL2 was mostly found in the intermediate phases of C/G-MS constructs. At eight weeks, however, the expression of COL2 was decreased by 36.5% than that at Week 1 ($p < 0.01$). The IHC results indicated the potential of spatial deposition of cartilaginous tissue in the C/G-MS constructs *in vivo*. In relation to inflammatory response, expression of the tissue macrophage surface marker CD68 of both implants was evaluated. Relatively high expression of CD68 was noted in the surrounding soft tissue of C/G-MS constructs at one week; by comparison, lower expression of CD68 was detected at four and eight weeks than at one week in C/G-MS constructs ($p < 0.05$). Markedly less CD68-immunopositive cells were found in cell-free scaffolds than in C/G-MS constructs at one and four weeks, respectively ($p < 0.01$ and $p < 0.05$).

Discussion

Complex tissue engineering has received great attention in the light of tremendous clinical needs. One challenge of engineering complex tissue is to create a biomimetic interface within an organ, especially between heterogeneous tissues such as soft and hard tissues [34]. Owing to four structurally continuous yet compositionally distinct tissue regions within the tendon-to-bone interface, the process of tissue engineering appeared to be more arduous. In particular, a multiphasic yet integrated scaffold is demanded, which is believed to be capable of recapitulating the multi-tissue organization observed at the native interface [8,9]. Spalazzi et al. [35,36] developed a continuous scaffold comprising three phases made from polyglactin (Phase A), poly(lactic-*co*-glycolic acid) (Phase B), and poly(lactic-*co*-glycolic acid)/bioactive glass composite (Phase C). Phases A, B, and C were intended for tendon, fibrocartilage, and bone regeneration, respectively. They were first manufactured separately and then sintered together by heating to form a triphasic scaffold, the process of which took days. The average height of the triphasic scaffold was 6 mm, which limits its clinical application as a biomimetic *ex vivo* graft, in that the human enthesis in the rotator cuff is no more than 1 mm. In our work, we managed to fabricate a biomimetic tendon-to-bone interface based on a much thinner 3D-printed multiphasic scaffold. The additive manufacturing technology not only provides rapid production via printing but also assures the integration and interconnectivity of the multiphasic scaffolds. The multihead 3D printing system used in this study allowed uninterrupted bottom-up printing from the biodegradable PCL phase mimicking the tendon to the osteoinductive PCL/TCP phase mimicking the bone. Based on histological fact that the fibrochondrocytes grow embedded in ECM, the intermediate phase was designed to have ample space for containing ECM-like hydrogels. Hence, the duct structure with one opening was designed for the intermediate phase, by which the cell-laden hydrogel could be easily injected to fill the certain space. Fibrocartilage is subjected to compressive loading in the native enthesis [5]. Biomechanical tests further demonstrated the suitable compressive modulus in the 3D-printed scaffolds during degradation, indicating the potential application in fibrocartilage regeneration in the enthesis. However, the 3D-printed scaffold produced in this study was still 2.5 mm in height, and further modification is required to cater for the small scale of the native enthesis.

GelMA is a photocurable hydrogel with remarkable cell-responsive and biodegradable properties. The rapid cross-linking ability makes it a commonly used cell-laden hydrogel. To seed heterotypic cells simultaneously, we loaded and photocrosslinked cell-laden GelMA on varying phases of the scaffold in a stratified manner. Cell seeding was accomplished in less than 2 min, by which a C/G-MS construct with graded cell types was fabricated. Within that, the maximum time of light exposure for cells encapsulated in GelMA was approximately 1 min, which had been demonstrated to have minor influence on cell viability in pilot studies. Cell proliferation and viability were further assessed to confirm cytocompatibility of the C/G-MS constructs *in vitro*. After seven days in culture, cellular microfilament staining demonstrated cells efficiently grew in GelMA hydrogels and on scaffold fibres (Figure 4A). We observed the cell morphology on both the top and intermediate phases; however, because the bottom (PCL) phase was very thin and only had two layers, we were unable to observe the cell stratum on this phase from the scaffold lateral by CLSM. Nevertheless, combining with the result of favourable cell viability on the PCL phase (Figure 3B), we confirmed good cytocompatibility on all three phases. Overall, we proved the GelMA-based cell seeding method was a facile and efficient approach for stratified cell seeding.

Normally, healing of the enthesis is achieved by the formation of fibrovascular tissue instead of regeneration of fibrocartilage. The loss of fibrocartilaginous insertion largely impairs its function in alleviating stress concentration and eventually hinders biomechanical transduction. Therefore, chondrogenesis of the biomimetic tendon-to-bone interface became the major research goal in our study. We evaluated the chondrogenic potential of the C/G-MS constructs both *in vitro* and *in vivo*. After three weeks of chondrogenic induction with the consistent addition of TGFβ3, expression of COL2 was detected by ICC analysis, and positive green fluorescence was identified in both GelMA hydrogels and scaffold fibres within the intermediate phase mimicking fibrocartilage (Figure 4B). It confirms BMSCs exhibited chondrogenic differentiation in the C/G-MS constructs after induction with TGFβ3. On the contrary, the same batch of C/G-MS constructs did not show a tendency of chondrogenesis after being cultured in the same media but without treating with TGFβ3. It was highly hypothesized that the FBs, BMSCs, and OBs in close proximity would enhance chondrogenic differentiation of BMSCs or even induce transdifferentiation of FBs [9,13]. For example, in the studies performed by Wang et al. [37,38], when cocultured with FBs and OBs, BMSCs showed significant fibrochondrogenic potential with increased proteoglycan production and TGFβ3 expression. In another study of the trilineage coculture system (OBs–BMSCs–FBs) on a hybrid silk scaffold, fibrocartilaginous differentiation of BMSCs was observed in both groups treated with or without TGFβ3 [24]. These studies drew a conclusion that the cell–cell physical contact and paracrine interaction might play an important role in promoting cell differentiation and influencing cellular phenotypes. Because we could not identify chondrogenesis in the C/G-MS constructs without treating with TGFβ3, there might be insufficient heterotypic cellular contact or lack of paracrine interaction in the coculture system. To address this issue, the cell seeding approach could be further optimized to enhance heterotypic cellular interactions. Besides, investigations on 3D-printed scaffolds or cell-laden GelMA equipped with biochemical cues in the intermediate phase to support sustained growth factor release are further needed.

To evaluate the biocompatibility and chondrogenesis of the C/G-MS constructs *in vivo*, we implanted them beneath the skin of mice. To evaluate the risk of inflammatory response induced by scaffold implantation, we detected expression of CD68 in the surrounding soft tissue of both implants (Figure 7). Low expression of CD68 could be identified in cell-free scaffolds at eight weeks, indicating minor macrophage recruitment; and the result was consistent with the findings of H&E staining. It demonstrates the as-fabricated 3D-printed scaffolds retain low risk of inducing material-related inflammation. Moreover, expression of CD68 decreased statistically in the surrounding tissue of C/G-MS constructs from Week 4. That indicates the cell-seeded constructs underwent orderly inflammation, which was from macrophage recruitment during the early stage (Week 1) to homoeostasis restoration after four weeks. Decrease in the number of macrophages is essential; otherwise, the inflammatory response would be exacerbated and, with more tissue-damaging irritant produced, fibrotic tissues would be largely formed around the implants [39].

There is a complex interlocking zone between mineralized fibrocartilage and bone within the enthesis, which is considered a vital structure in anchoring the tendon to bone, for the interdigitation of

mineralized fibrocartilage can resist against shear force and ultimately minimize stress concentration [5]. COL10 is predominantly synthesized by hypertrophic chondrocytes in the process of endochondral bone formation; therefore, it is a typical collagen denoting the characteristic of hypertrophic chondrocytes. In this study, the distinct increasing pattern of *Col10* expression demonstrated the progressive formation of calcifying cartilage within the C/G-MS coculture system, which indicates regenerative potential of mineralized fibrocartilage (Figure 5D). Consequently, it may have beneficial effects on the formation of the complex interlocking structure and contribute to biomechanics of the enthesis.

During eight weeks of implantation, gene expression of tenogenic, chondrogenic, and osteogenic markers of the C/G-MS construct showed an overall increasing pattern (Figure 5). In addition, the C/G-MS construct exhibited a continuous but graded histological structure up to four weeks (Figure 6). The results of molecular and histological tests strongly indicated the potential of the C/G-MS construct to regenerate a heterogeneous tissue and integrate with both the tendon and bone. Before fabrication, BMSCs were cultured in TGFβ3-supplemented media for three weeks. TB and SO/FG staining methods successfully identified the distinct proteoglycan distribution in the intermediate (fibrocartilage) phase at one week after implantation. However, both staining subsided significantly from four to eight weeks, indicating less chondrocytes differentiated from BMSCs without sustained chondrogenic induction. The results were further confirmed by immunolocalizing COL2 (Figure 7). Expression of COL2 was mostly found in the intermediate phase and decreased by 36.5% at eight weeks than at one week. Subcutaneous implantation may account for the unsustainable chondrogenesis after four weeks, for the subcutaneous physiological environment is quite different from the enthesis. Therefore, although the ectopic implantation yielded meaningful outcomes, it is still a limitation to this study. In addition, to explore the optimization of the scaffolds for sustained chondrogenic induction, a healing model with the biomimetic interface implanted in the native enthesis of the rotator cuff is demanded and worthy of research. To this end, the size and structure of the 3D-printed scaffold should be customized based on the anatomical characteristic of the enthesis of the selected large animal model.

Another limitation of this study is that mechanical stimuli were not involved in current strategies for interface tissue engineering. Formation of a functionally graded tendon-to-bone interface requires biomechanical loading [8]. However, the mechanobiology of enthesis development and interface healing has not been fully elucidated, which hinders a strategy involving application of biophysical cues.

Conclusion

In summary, a biomimetic tendon-to-bone interface was fabricated, and its biocompatibility and chondrogenesis were evaluated both *in vitro* and *in vivo*. The use of 3D-printed multiphasic scaffolds and GelMA-based stratified cell seeding approach were demonstrated to be effective strategies for heterogeneous interface tissue engineering. Future work will focus on the optimization of 3D-printed scaffolds, the adjustment of cell seeding approach, and the healing potential after implantation of the biomimetic interface in the enthesis of a large animal model.

Conflict of interest

The authors have no conflicts of interest to disclose in relation to this article.

Funding/support statement

This work was supported by the grants from the National Natural Science Foundation of China (nos. 81620108019, 81571944) and from the Shanghai Science and Technology Committee (18511109602).

Appendix A. Supplementary data

Supplementary data to this article can be found online at https://doi.org/10.1016/j.jot.2020.01.004.

References

[1] Lui P, Zhang P, Chan K, Qin L. Biology and augmentation of tendon-bone insertion repair. J Orthop Surg Res 2010;5:59.
[2] Atesok K, Fu FH, Wolf MR, Ochi M, Jazrawi LM, Doral MN, et al. Augmentation of tendon-to-bone healing. J Bone Joint Surg Am 2014;96:513–21.
[3] Greenspoon JA, Petri M, Warth RJ, Millett PJ. Massive rotator cuff tears: pathomechanics, current treatment options, and clinical outcomes. J Shoulder Elbow Surg 2015;24:1493–505.
[4] Patel S, Gualtieri AP, Lu HH, Levine WN. Advances in biologic augmentation for rotator cuff repair. Ann N Y Acad Sci 2016;1383:97–114.
[5] Benjamin M, Kumai T, Milz S, Boszczyk BM, Boszczyk AA, Ralphs JR. The skeletal attachment of tendons–tendon "entheses". Comp Biochem Physiol A Mol Integr Physiol 2002;133:931–45.
[6] Apostolakos J, Durant TJ, Dwyer CR, Russell RP, Weinreb JH, Alaee F, et al. The enthesis: a review of the tendon-to-bone insertion. Muscles Ligaments Tendons J 2014;4:333–42.
[7] Rothrauff BB, Tuan RS. Cellular therapy in bone-tendon interface regeneration. Organogenesis 2014;10:13–28.
[8] Lu HH, Thomopoulos S. Functional attachment of soft tissues to bone: development, healing, and tissue engineering. Annu Rev Biomed Eng 2013;15:201–26.
[9] Boys AJ, McCorry MC, Rodeo S, Bonassar LJ, Estroff LA. Next generation tissue engineering of orthopedic soft tissue-to-bone interfaces. MRS Commun 2017;7:289–308.
[10] Langer R, Vacanti JP. Tissue engineering. Science 1993;260:920–6.
[11] Yousefi AM, Hoque ME, Prasad RG, Uth N. Current strategies in multiphasic scaffold design for osteochondral tissue engineering: a review. J Biomed Mater Res A 2015;103:2460–81.
[12] Kang H, Zeng Y, Varghese S. Functionally graded multilayer scaffolds for in vivo osteochondral tissue engineering. Acta Biomater 2018;78:365–77.
[13] Smith L, Xia Y, Galatz LM, Genin GM, Thomopoulos S. Tissue-engineering strategies for the tendon/ligament-to-bone insertion. Connect Tissue Res 2012;53:95–105.
[14] Atesok K, Doral MN, Karlsson J, Egol KA, Jazrawi LM, Coelho PG, et al. Multilayer scaffolds in orthopaedic tissue engineering. Knee Surg Sports Traumatol Arthrosc 2016;24:2365–73.
[15] Mok SW, Nizak R, Fu SC, Ho KK, Qin L, Saris DBF, et al. From the printer: potential of three-dimensional printing for orthopaedic applications. J Orthop Translat 2016;6:42–9.
[16] Gleadall A, Visscher D, Yang J, Thomas D, Segal J. Review of additive manufactured tissue engineering scaffolds: relationship between geometry and performance. Burns Trauma 2018;6:19.
[17] Merceron TK, Burt M, Seol YJ, Kang HW, Lee SJ, Yoo JJ, et al. A 3D bioprinted complex structure for engineering the muscle-tendon unit. Biofabrication 2015;7:035003.
[18] Yang G, Lin H, Rothrauff BB, Yu S, Tuan RS. Multilayered polycaprolactone/gelatin fiber-hydrogel composite for tendon tissue engineering. Acta Biomater 2016;35:68–76.
[19] Nyberg E, Rindone A, Dorafshar A, Grayson WL. Comparison of 3D-printed poly-ε-caprolactone scaffolds functionalized with tricalcium phosphate, hydroxyapatite, bio-oss, or decellularized bone matrix. Tissue Eng 2017;23:503–14.
[20] Rai B, Lin JL, Lim ZX, Guldberg RE, Hutmacher DW, Cool SM. Differences between in vitro viability and differentiation and in vivo bone-forming efficacy of human mesenchymal stem cells cultured on PCL-TCP scaffolds. Biomaterials 2010;31:7960–70.
[21] Yu W, Li R, Long J, Chen P, Hou A, Li L, et al. Use of a three-dimensional printed polylactide-coglycolide/tricalcium phosphate composite scaffold incorporating magnesium powder to enhance bone defect repair in rabbits. J Orthop Translat 2018;16:62–70.
[22] Font Tellado S, Balmayor ER, Van Griensven M. Strategies to engineer tendon/ligament-to-bone interface: biomaterials, cells and growth factors. Adv Drug Deliv Rev 2015;94:126–40.
[23] Calejo I, Costa-Almeida R, Gomes ME. Cellular complexity at the interface: challenges in enthesis tissue engineering. Adv Exp Med Biol 2019;1144:71–90.
[24] He P, Ng KS, Toh SL, Goh JC. In vitro ligament-bone interface regeneration using a trilineage coculture system on a hybrid silk scaffold. Biomacromolecules 2012;13:2692–703.
[25] Zhu C, Pongkitwitoon S, Qiu J, Thomopoulos S, Xia Y. Design and fabrication of a hierarchically structured scaffold for tendon-to-bone repair. Adv Mater 2018;30:1707306.
[26] Nichol JW, Koshy ST, Bae H, Hwang CM, Yamanlar S, Khademhosseini A. Cell-laden microengineered gelatin methacrylate hydrogels. Biomaterials 2010;31:5536–44.
[27] Kaemmerer E, Melchels FP, Holzapfel BM, Meckel T, Hutmacher DW, Loessner D. Gelatine methacrylamide-based hydrogels: an alternative three-dimensional cancer cell culture system. Acta Biomater 2014;10:2551–62.
[28] Zhang X, Li J, Ye P, Gao G, Hubbell K, Cui X. Coculture of mesenchymal stem cells and endothelial cells enhances host tissue integration and epidermis maturation through AKT activation in gelatin methacryloyl hydrogel-based skin model. Acta Biomater 2017;59:317–26.

[29] Zhang J, Wang JH. Characterization of differential properties of rabbit tendon stem cells and tenocytes. BMC Muscoskel Disord 2010;11:10.
[30] Bakker AD, Klein-Nulend J. Osteoblast isolation from murine calvaria and long bones. Methods Mol Biol 2012;816:19–29.
[31] Soleimani M, Nadri S. A protocol for isolation and culture of mesenchymal stem cells from mouse bone marrow. Nat Protoc 2009;4:102–6.
[32] Xie M, Gao Q, Zhao H, Nie J, Fu Z, Wang H, et al. Electro-assisted bioprinting of low-concentration GelMA microdroplets. Small 2019;15:e1804216.
[33] Tuli R, Tuli S, Nandi S, Wang ML, Alexander PG, Haleem-Smith H, et al. Characterization of multipotential mesenchymal progenitor cells derived from human trabecular bone. Stem Cell 2003;21:681–93.
[34] Atala A, Kasper FK, Mikos AG. Engineering complex tissues. Sci Transl Med 2012;4:160rv12.
[35] Spalazzi JP, Doty SB, Moffat KL, Levine WN, Lu HH. Development of controlled matrix heterogeneity on a triphasic scaffold for orthopedic interface tissue engineering. Tissue Eng 2006;12:3497–508.
[36] Spalazzi JP, Dagher E, Doty SB, Guo XE, Rodeo SA, Lu HH. In vivo evaluation of a multiphased scaffold designed for orthopaedic interface tissue engineering and soft tissue-to-bone integration. J Biomed Mater Res A 2008;86:1–12.
[37] Wang IE, Shan J, Choi R, Oh S, Kepler CK, Chen FH, et al. Role of osteoblast-fibroblast interactions in the formation of the ligament-to-bone interface. J Orthop Res 2007;25:1609–20.
[38] Wang IE, Bogdanowicz DR, Mitroo S, Shan J, Kala S, Lu HH. Cellular interactions regulate stem cell differentiation in tri-culture. Connect Tissue Res 2016;57:476–87.
[39] Murray PJ, Wynn TA. Protective and pathogenic functions of macrophage subsets. Nat Rev Immunol 2011;11:723–37.